

See discussions, stats, and author profiles for this publication at: <https://www.researchgate.net/publication/51881626>

# Photophysical Properties and Photochemistry of EE-, EZ-, and ZZ-1, 4-Dimethoxy-2,5-bis[2-(thien-2-yl)ethenyl] Benzene in Solution: Theory and Experiment

ARTICLE *in* THE JOURNAL OF PHYSICAL CHEMISTRY A · DECEMBER 2011

Impact Factor: 2.69 · DOI: 10.1021/jp206463k · Source: PubMed

---

CITATIONS

4

READS

16

---

## 6 AUTHORS, INCLUDING:



[Songwut Suramitr](#)

Kasetsart University

17 PUBLICATIONS 119 CITATIONS

[SEE PROFILE](#)



[Peter Wolschann](#)

University of Vienna

228 PUBLICATIONS 2,149 CITATIONS

[SEE PROFILE](#)



[Masahiro Ehara](#)

Institute for Molecular Science

201 PUBLICATIONS 4,717 CITATIONS

[SEE PROFILE](#)



[Supa Hannongbua](#)

Kasetsart University

175 PUBLICATIONS 1,381 CITATIONS

[SEE PROFILE](#)

# Photophysical Properties and Photochemistry of *EE*-, *EZ*-, and *ZZ*-1,4-Dimethoxy-2,5-bis[2-(thien-2-yl)ethenyl] Benzene in Solution: Theory and Experiment

Songwut Suramitr,<sup>\*,†,‡</sup> Suphawarat Phalinyot,<sup>†,‡</sup> Peter Wolschann,<sup>§</sup> Ryoichi Fukuda,<sup>⊥,♯</sup> Masahiro Ehara,<sup>⊥,♯</sup> and Supa Hannongbua<sup>†,‡</sup>

<sup>†</sup>Department of Chemistry, Faculty of Science and <sup>‡</sup>The Center of Nanotechnology KU, Kasetsart University, Bangkok 10900, Thailand

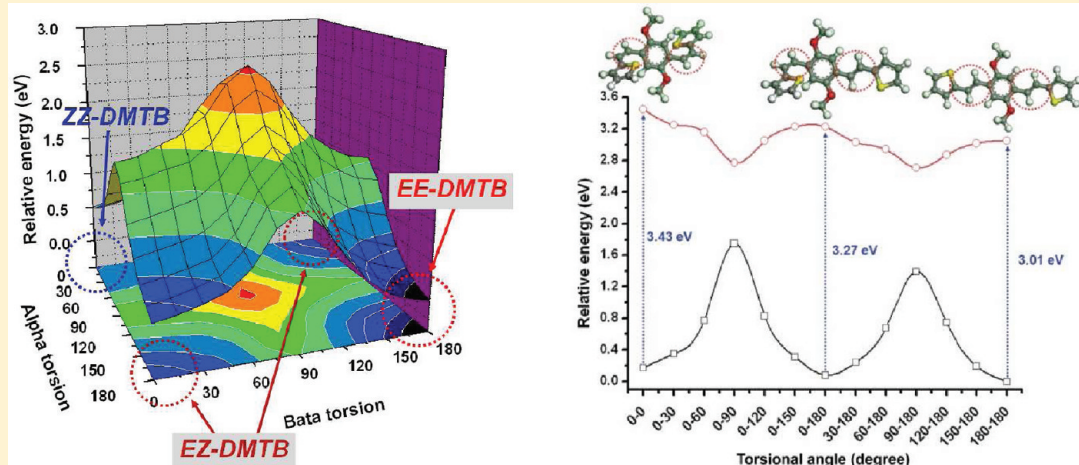
<sup>§</sup>Institute for Theoretical Chemistry, University of Vienna, Währinger Straße 17 A-1090 Vienna, Austria

<sup>⊥</sup>Institute for Molecular Science and Research Center for Computational Science, 38 Nishigo-naka, Myodaiji, Okazaki 444-8585, Japan

<sup>#</sup>Japan Science and Technology Agency CREST, Sanboncho-5, Chiyoda-ku, Tokyo 102-0075, Japan

Supporting Information

## ABSTRACT:



Photophysical properties and photoisomerization of 1,4-dimethoxy-2,5-bis[2-(thien-2-yl)ethenyl] benzene (DMTB) have been investigated for the *EE*-, *EZ*-, and *ZZ*-stereoisomers. The *EE*-DMTB was prepared, and the absorption/fluorescence spectra of *EE*-isomer as well as transient spectra in photoisomerization among three isomers were observed. Absorption and fluorescence spectra of three isomers were analyzed by the symmetry-adapted cluster-configuration interaction (SAC–CI) and time-dependent density functional theory (TDDFT) methods. The characteristics of the absorption spectra of three isomers were satisfactorily reproduced by the direct SAC–CI and TDDFT methods in both peak position and intensity. The relative stability of three isomers and the photoisomerization among these isomers were also examined theoretically. The ground ( $S_0$ ) and first excited state ( $S_1$ ) geometries were calculated by the DFT/TDDFT method with the M06HF functional, and the calculated  $S_0$  structures of *EE*- and *ZZ*-isomers agreed well with those of the X-ray structures. The geometry relaxation in the  $S_1$  state was interpreted with regard to the excitation character. The solvent effect in the absorption and fluorescence spectra was examined by the polarizable continuum model (PCM) and was found to be 0.05–0.20 eV, reflecting the charge polarization. The results show that the photophysical properties of DMTB can be controlled with the conformation constraint and also indicate the possibility of a photofunctional molecular device such as a switching function.

## 1. INTRODUCTION

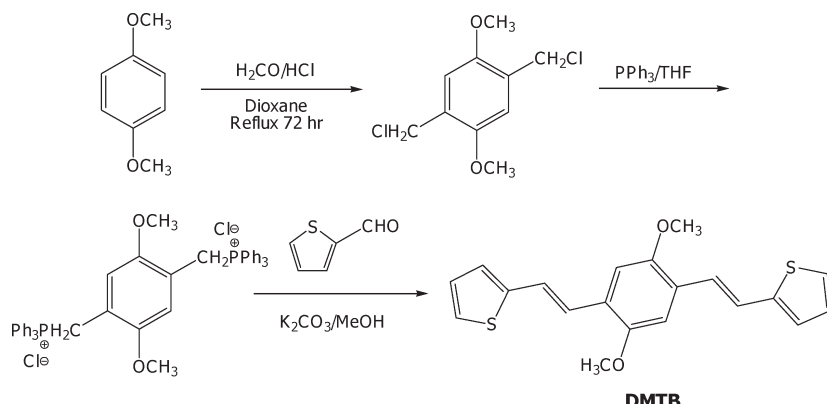
Optical properties as well as electrochemical and conductive properties of the conjugated molecules have received extensive attention in the field of material chemistry of electronic devices such as light-emitting diodes (LEDs), field effect transistors (FETs), and photovoltaic cells (PCs). Various types of organic molecules including heteroatoms in  $\pi$ -conjugation have been

developed, and their characteristic electronic structure provides attractive photophysical properties and rich photochemistry.<sup>1–4</sup> Some of these conjugated molecules are also of fundamental

Received: July 8, 2011

Revised: November 21, 2011

Published: December 15, 2011

**Scheme 1.** Three-Step Synthesis of DMTB

interest in view of molecular devices, taking advantage of their characteristic properties in the excited states. Theoretical information on the energetics and molecular properties in the excited states is variable for the development of the photofunctional molecules of desirable photophysical properties.

Among the category of  $\pi$ -conjugated polymer materials including heteroatoms, the 1,4-dialkoxy-2,5-bis[2-(thien-2-yl)ethenyl]benzene (DATB) unit is of interest because it can be regarded as a derivative of poly phenylenevinylene (PPV), which achieves high quantum yield of electroluminescence. The DATB has three structural isomers, namely, *EE*-, *EZ*-, and *ZZ*- isomers, which exhibit different photophysical properties in absorption and fluorescence. This implies that it is also of interest to control the photophysical properties of DATB and its derivatives and also to examine the possibility of photochemical functions as molecular devices.

Recently, the photochemistry and electrochemistry of DATB were investigated by Waskiewicz et al.<sup>5</sup> In their work, the photoisomerization at the ethenyl double bonds was focused since it is relevant to the photophysical property because the nonradiative decay to the ground ( $S_0$ ) state competes with the fluorescence; the absorption spectra of these three isomers were observed, and the photoisomerization among these isomers was monitored. The absorption spectra, however, were not theoretically analyzed, although the ground-state structure was examined by the AM1 method. The absorption spectra of 1,4-diethoxy-2,5-bis[2-(thien-2-yl)ethenyl]benzene (DMTB) were also studied with the time-dependent (TD) density functional theory (DFT) calculations by Fuks-Janczarek et al.<sup>6</sup> The agreement between the theoretical and experimental spectra, however, was not satisfactory for the higher excited states. Therefore, the detailed assignments of the spectra are necessary to understand the photophysical properties and photochemistry of DMTB in three stereoisomers. In particular, the emission properties and excited-state structure of these isomers that are relevant for photofunctional molecules have not been investigated, to our best knowledge.

Theoretical investigations of the absorption and emission spectra by means of quantum chemical calculations have nowadays become a standard approach, being widely used to help assignment of the experimental spectra and gain insights into the underlying electronic structure and photochemistry. TDDFT has become popular due to its low computational cost and increasing reliability in calculating excited states.<sup>7–12</sup> The method has been successfully applied to various types of molecular

excited states. Previously, we investigated the photophysical properties of organic light-emitting diode (OLED) molecules such as PPV, polycarbazoles, and polyfluorenes, by the TDDFT calculations.<sup>13–17</sup>

The symmetry-adapted cluster-configuration interaction (SAC–CI) method<sup>18–21</sup> has been established as a useful and reliable tool to investigate the molecular excited states. The method has been successfully applied to wide varieties of molecular excited states in organic and inorganic molecules.<sup>22,23</sup> Therefore, it can be also used to confirm the accuracy of TDDFT calculations, which are subject to functional dependences. By the SAC–CI method, we have investigated the photophysical properties of numerous  $\pi$ -conjugated molecules. They include the absorption/emission spectra and molecular geometry in excited states of OLED molecules<sup>24–26</sup> and the photochemistry of the ultraviolet B blocking molecules.<sup>27</sup> In those works, the electronic spectra were well reproduced with the reliable assignments proposed, and the color tuning by introducing substituents was also examined satisfactorily.

We have studied the absorption and emission spectra and excited-state geometries of PPV and poly-*para*-phenylene (PP) by the SAC–CI method. This study shows that conventional TDDFT should be used carefully for long  $\pi$ -conjugating molecules. Computational studies with the DFT/TDDFT associated with the SAC–CI calculations can be helpful to investigate photochemical and photophysical properties of relatively large  $\pi$ -conjugating molecules. It should be noted that the direct algorithm of the SAC–CI method has been recently developed,<sup>28</sup> and this method has enabled accurate and efficient calculations, in particular, for large systems.<sup>29</sup> The present study also shows an example for the excited states of large  $\pi$ -conjugating molecules using ab initio and DFT calculations.

The solvent effects on the absorption and emission spectra are also relevant; therefore, we estimated the solvent effect on electronic spectra with a continuum solvent model in this study. The polarizable continuum model (PCM) is one of the most common and effective models among theoretical methods for considering solvent effects.<sup>30</sup> It can provide conceptually simple but accurate and physically well-founded descriptions of solvent effects in several molecular properties. In the calculations of absorption and emission spectra with the PCM, we have to consider the solvent effect on both the ground and excited states by a proper scheme. The state-specific solvation approach with a nonequilibrium solvation scheme provides a proper description of the fast electron transition process in

solvent circumstances.<sup>31–35</sup> The PCM is applicable to large systems due to its low computational cost and can be combined with high-level electronic structure theory. Thus, the TDDFT method combined with PCM<sup>34–36</sup> has been developed and applied to various systems. Recently, PCM has been combined with the SAC–CI method to calculate the solvation free energy in excited states, and its analytical energy gradients have also been developed.<sup>37,38</sup>

In this paper, we theoretically investigate the absorption and fluorescence spectra of DMTB in the three isomers, *EE*, *EZ*- and *ZZ*. We also synthesized the *EE*-DMTB isomer and observed the absorption and fluorescence spectra in chloroform as well as the transient electronic spectra in photoisomerization among these isomers. We applied the direct SAC–CI and TDDFT methods to provide a reliable assignment of the absorption spectra in a wide energy range and to clarify the characteristic spectra of three isomers. The ground- and excited-state geometries were calculated and discussed in comparison to the X-ray structures. The solvent effect on the absorption and emission spectra was analyzed by the charge reorganization caused by the excitation. In addition, the relative stability of the three isomers and the photochemistry of the cis–trans isomerization were also examined.

## 2. EXPERIMENTAL AND COMPUTATIONAL DETAILS

**2.1. Synthesis and Characterization.** The DMTB ( $C_{20}H_{18}O_2S_2$ ) was synthesized according to the conventional procedure described in the literature, as shown in Scheme 1.<sup>5,6</sup> The 1,4-dimethoxy benzene was chloromethylated with formaldehyde and HCl in dioxane solution. The reaction product then was treated with triphenylphosphine to produce the corresponding salt, which was directly used for the Wittig's reaction with 2-thienylcarboaldehyde in potassium carbonate/dry methanol to give the product of DMTB as a pale-yellow oil after chromatographic purification. This compound was confirmed by  $^1H$ -NMR (nuclear magnetic resonance),  $^{13}C$ -NMR, and FTIR (Fourier transform infrared spectroscopy), referring to the reported data.<sup>3</sup>

The UV-vis measurement was done with Perkin-Elmer Lambda 35 UV-vis spectrophotometer using a quartz cell with a 1 cm path length. The fluorescence spectrum was obtained using a Perkin-Elmer Instruments LS55 fluorescence spectrophotometer. All measurements were carried out at 25 °C in chloroform solution.

**2.2. Ground- and Excited-State Calculations.** To calculate the absorption and emission spectra, the geometry optimizations were performed for the ground ( $S_0$ ) and first singlet excited ( $S_1$ ) states for three isomers, *EE*, *EZ*, and *ZZ*-DMTB, shown in Figure 1. The ground-state geometries were optimized by DFT with B3LYP,<sup>39–41</sup> PBE0,<sup>42,43</sup> and M06HF<sup>44</sup> functionals. We also performed MP2 (the second-order Møller–Plesset perturbation theory) calculations to confirm the accuracy of the DFT results. The basis set dependence of the results was also examined, and the results were complied in Supporting Information. We used the M06HF/D95(d)<sup>45</sup> geometry because it reasonably reproduced the experimental molecular structure.

Using these geometries in the ground state, the excitation energies were examined, and we found that the geometry dependence of the calculated excitation energies was not so significant in the preliminary calculations. Thus, we adopted the geometries optimized by the DFT(M06HF) method with the D95(d) basis<sup>45</sup> to consider the computational costs and consistency. The optimized structures of *EE*, *EZ*, and *ZZ*-DMTB

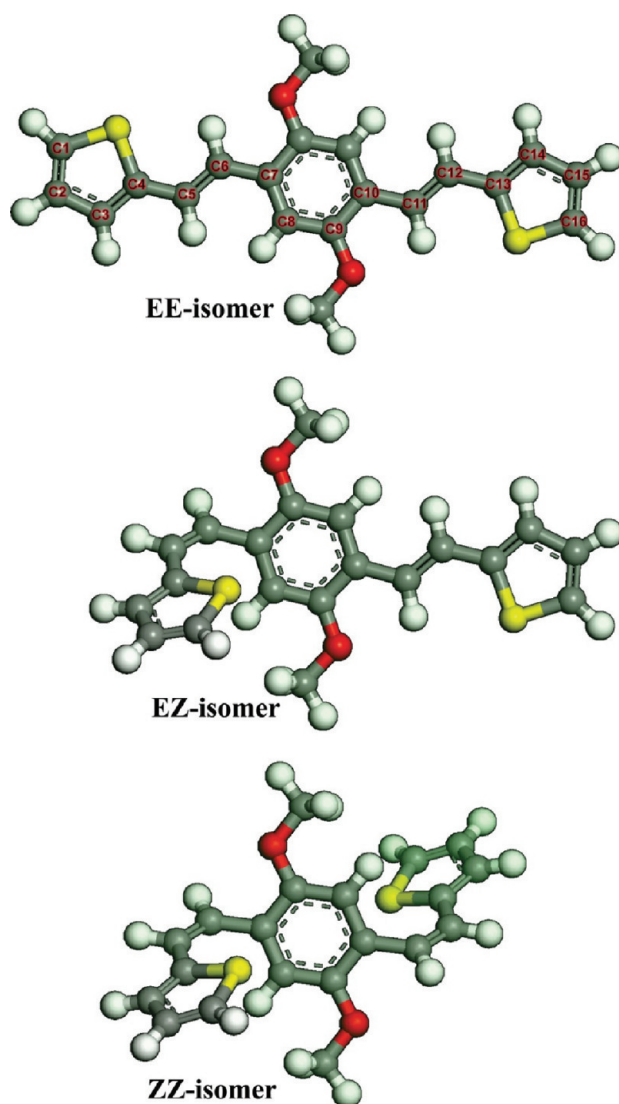


Figure 1. Molecular structures of *EE*-, *EZ*-, and *ZZ*-DMTB and the atom number on the backbone in *EE*-DMTB.

isomers belong to  $C_{2h}$ ,  $C_1$ , and  $C_i$  point groups, respectively. These structures were confirmed to be local minima by the vibrational frequency analysis.

The molecular geometries in the  $S_1$  state, which corresponds to the  $\pi \rightarrow \pi^*$  transition, were optimized by the TDDFT-(M06HF)/D95(d) scheme with the initial geometries taken from the ground-state ones. We performed vibrational frequency analysis of the  $S_1$  state by CIS (configuration interaction with single excitations) calculations, and we found that the  $C_{2h}$  structure of the *EE*- isomer is a local minimum, but the  $C_1$  structure of the *ZZ*- isomer has one imaginary vibrational mode. Therefore, the optimized  $C_i$  structure of the *ZZ*- isomer is a quasi-stable structure. In this study, we assumed that the fluorescence maxima correspond to the emission from the energy minimum of the lowest excited state restricted by the symmetry of the ground state. We did not perform further geometry optimization for the *ZZ*- isomer in lower symmetry because it would lead to the photoisomerization processes. The emission process would compete with the photoisomerization, and this is discussed in the subsequent section.

The electronic excitation energies and oscillator strengths were calculated using the TDDFT and SAC–CI methods at the molecular structures optimized by TDDFT(M06HF). To simulate the absorption spectra, the low-lying singlet excited states in the energy region below  $\sim 5.5$  eV ( $\sim 200$  nm) were examined. The TDDFT calculations were performed with three different functionals to examine the functional dependence. Standard hybrid functionals B3LYP and PBE0 were employed in the calculations. The CAM (Coulomb-attenuating method) B3LYP<sup>46</sup> was also examined to take into account the long-range corrections for describing the long  $\pi$ -conjugation. Standard exchange functionals may suffer from improper long-range description, in particular, for the electronic excited states of significantly different polarity between the ground and excited states.<sup>44</sup>

In the SAC/SAC–CI calculations, the singles and doubles (SD)-R method with the direct calculation of the  $\sigma$  vector, that is, the direct SAC–CI variational approach,<sup>28</sup> was used with CIS vectors as initial guess. Therefore, low-lying double-electron excited states that may exist in large  $\pi$ -conjugated systems were not calculated in this study. The perturbation selection technique<sup>47</sup> was used to reduce the computational cost. The threshold of the double excitation operators for SAC ( $S_2$  operators) was set to  $\lambda_g = 5.0 \times 10^{-6}$ , and that of the double excitation operators for the SAC–CI excited states ( $R_2$  operators) was set to  $\lambda_e = 5.0 \times 10^{-7}$ . All of the product terms generated by the  $S_2S_2$ ,  $R_1S_2$ , and  $R_2S_2$  operators were included in the direct SAC–CI calculations, where  $R_1$  denotes the singly excited operators in the SAC–CI.<sup>28</sup>

**2.3. Effect of Solvent on Electronic Properties.** The solvent effect on both the geometries and transition energies has been evaluated by means of the PCM. The integral equation formula (IEF) PCM with the default parameters of GAUSSIAN 09 was used for the present calculations.<sup>48</sup> The calculations were performed in vacuum (without PCM) and in chloroform ( $\text{CHCl}_3$ ) with PCM.

Electronic transitions are much faster processes than the conformational and orientational changes of solvent molecules. Therefore, not all degrees of freedom of the solvent determining the solvent polarization are able to respond to the sudden variation of the solute charge distribution caused by electronic transition. In the PCM, a nonequilibrium solvation scheme has been developed to describe electronic transitions in solution.<sup>49</sup> In the nonequilibrium solvation scheme, the static dielectric constant of a solvent ( $\epsilon_0$ ) is divided into dynamic ( $\epsilon_{\text{dyn}}$ ) and inertial ( $\epsilon_{\text{in}}$ ) parts as

$$\epsilon_0 = \epsilon_{\text{dyn}} + \epsilon_{\text{in}} \quad (1)$$

Consequently, the solvent polarization  $P$  can be divided into  $P_{\text{dyn}}$  and  $P_{\text{in}}$ . The polarization  $P_{\text{dyn}}$  responds fast to the solute charge distribution, and therefore, it is determined by the final state (after electron transition) of the solute molecule. On the other hand, the polarization  $P_{\text{in}}$  is a slow part and remains in the solvation for the initial state (before electron transition) of the solute charge distribution. For absorption spectra, the ground and excited states are the initial and final states, respectively.

There are two solvation schemes possible for calculating excitation energies using the methods based on the linear response (LR) theory, such as random phase approximation (RPA), TDDFT, SAC–CI, and LR coupled-cluster (CC). The first scheme is the state-specific (SS) solvation in which the

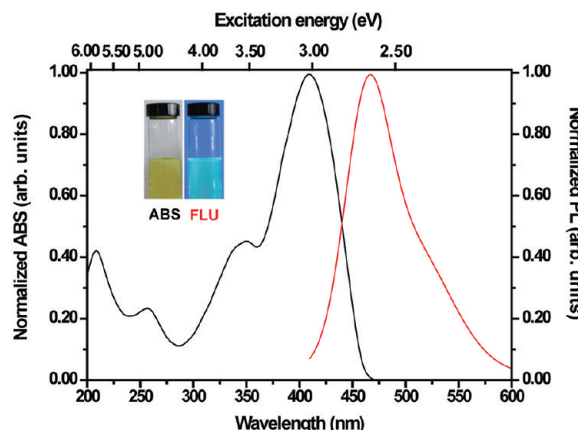


Figure 2. Absorption (Abs) and fluorescence (Flu) spectra of EE-DMTB in chloroform solution.

solvent polarization charges are determined by the electron density of the solute in the specific excited state. Consequently, the calculations are nonlinear, and each state is calculated by means of the self-consistent reaction field (SCRF) scheme. The second scheme is LR solvation in which solvent polarization charges are fixed in the ground state. Therefore, in the LR solvation scheme, the electron densities of the excited states are not necessary, and excitation energies can be calculated without additional iterations. It has been pointed out that the LR and SS schemes are intrinsically different for the solvent effect on excitation energies, and the SS scheme is more reliable in principle.<sup>30,31,33,50</sup> In this study, we used both the SS and LR solvation schemes of the PCM in the TDDFT calculations.<sup>33–35</sup>

For absorption, the molecular geometry in chloroform was optimized for the  $S_0$  state with equilibrium solvation, and the TDDFT calculations were performed with the SS and LR solvation schemes in the nonequilibrium model. For emission, the  $S_1$  state geometry in chloroform was optimized with equilibrium solvation and the LR scheme. Then, the excitation energies were calculated with the SS and LR solvation schemes in the nonequilibrium model. All calculations were performed using the GAUSSIAN 09 suite<sup>48</sup> of programs, revision B.01.

### 3. RESULTS AND DISCUSSION

**3.1. UV–Vis Absorption and Fluorescence Spectra.** The observed UV–vis and fluorescence spectra of EE-DMTB are shown in Figure 2. The maximum absorption ( $\lambda_{\text{max}}$ ) of EE-DMTB is 416 nm (2.98 eV), whereas the peak maximum of fluorescence is 458 nm (2.71 eV); the stokes shift is 42 nm (0.27 eV). This indicates that the structure relaxation in the  $S_1$  state is small and the main chain structure is rigid for the electronic excitation. As seen in the inset of Figure 2, the EE-DMTB exhibits blue emission. This blue emission may be of interest as a new source of luminescence material in the fabrication of OLED-based products. The absorption spectrum of EE-DMTB measured in chloroform shows a strong absorption centered at 416 nm (2.98 eV) and two intense peaks at 355 and  $\sim 210$  nm (3.49 and 5.90 eV) with the shoulder at 262 nm (4.73 eV). The observed spectrum is in accordance with that from the previous study.<sup>5</sup> The photoisomerization process of DMTB stereoisomers can be observed when the EE-, EZ-, or ZZ- isomer in solution is exposed to UV radiation. The EE-DMTB solution ( $10^{-4}$  M) was

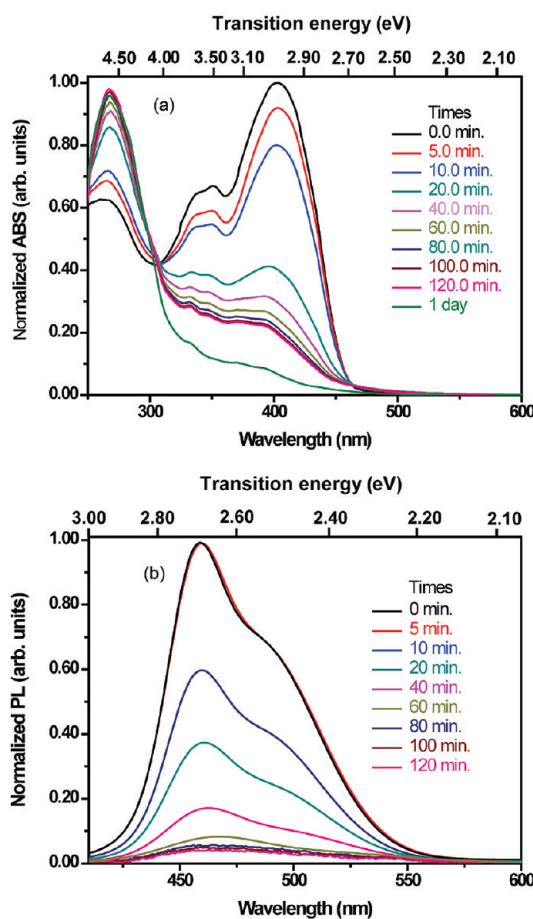


**Figure 3.** (a) UV-vis absorption and (b) fluorescence spectra of DMTB in chloroform solution after UV irradiation from 0 to 120 min (1 day for absorption).

used for UV irradiation analysis. The *EE*-DMTB solution was irradiated by the light source (broad spectrum 200–400 nm UV lamp) to result in a  $29.0 \text{ W cm}^{-2}$  UV power exposure at  $25^\circ\text{C}$  for 2 h. The UV-vis and fluorescence spectra were recorded for each sample with different UV irradiation times. Data were collected over the 200–600 nm range. The transient UV-vis absorption and fluorescence spectra measured in chloroform are shown in Figure 3. As will be discussed later, the absorption spectra of *EE*-, *EZ*-, and *ZZ*- isomers have peak maxima at 416, 377, and 345 nm, respectively. On the basis of this fact, the transient UV-vis spectra show photoisomerization among *EE*-, *EZ*-, and *ZZ*-DMTB clearly. In contrast, the transient fluorescence spectra show monotonic change, and the photoisomerization can be seen by the change of fluorescence intensity. These results indicate that the transient UV-vis absorption spectra are useful to monitor the photoisomerization and alternatively detect the intermediate products that are identified here evidently as *EZ*- and *ZZ*- isomers.

In the fluorescence spectrum, the course of the photoisomerization process may also be demonstrated in terms of the fluorescence quantum yield. The fluorescence quantum yield measured for the DMTB solutions exposed to UV radiation with different irradiation times is shown in Figure 4. The fluorescence quantum yield of the DMTB was measured at room temperature by a relative method using quinine sulfate in sulfuric acid as a

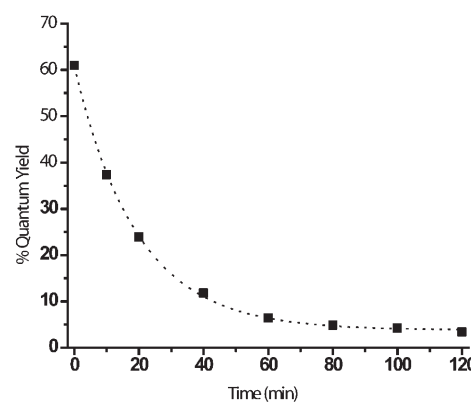


**Figure 4.** Fluorescence quantum yield (%) after the irradiation time of DMTB in chloroform solution.

standard. The fluorescence quantum yield  $\phi$  was calculated by

$$\phi_s = \phi_r \frac{F_s}{F_r} \frac{A_r}{A_s} \left( \frac{n_r}{n_s} \right)^2 \quad (2)$$

where  $F$  is the integration of the fluorescence intensities,  $n$  is the index of reflection of the solution,  $A$  is the absorbance at the excitation wavelength, and the subscripts  $r$  and  $s$  denote the reference and unknown sample, respectively.

The observed fluorescence quantum yield indicates the photoisomerization of the *EE*- isomer to *EZ*- or *ZZ*- isomers. The rate of the fluorescence change of the *EE*-DMTB isomer is fitted as  $y = 56.93 \exp(-t/19.37) + 3.81$ . This indicates that the fluorescence monitoring of the photoisomerization is possible due to the different fluorescence intensity of three isomers. The mechanism of the isomerization of DMTB has not been fully understood, although it was postulated that the isomerization process is accompanied by fast consecutive reactions. To discuss this issue, quantum chemical calculations were used to examine the photoisomerization processes in section 3.2.

**3.2. Ground- and Excited-State Calculations.** 3.2.1. Geometries in the  $S_0$  and  $S_1$  States of *EE*-, *EZ*-, and *ZZ*-DMTB. The molecular structures of three isomers in the  $S_0$  and  $S_1$  states were obtained by the DFT/TDDFT(M06HF) method. The optimized bond lengths and torsion angles in these states are summarized in Table 1 with the X-ray crystallographic data for the *EE*- and *ZZ*-DMTB isomers.<sup>51</sup> In Figure 5, the C–C bond lengths along the main chain are compared for the *EE*-, *EZ*-, and *ZZ*-DMTB isomers based on the optimized geometries in the  $S_0$  and  $S_1$  states.

The ground-state structure of the *EE*-DMTB isomer is planar due to the  $\pi$ -conjugation, while those of other two isomers are nonplanar with the dihedral angle  $\angle \text{C5-C6-C7-C8}$  being  $\sim 50^\circ$  because of the steric repulsion, as shown in Table 1. The X-ray structures were reported for the *EE*-DMTB and *ZZ*-DMTB isomers.<sup>51</sup> The geometrical parameters calculated by the DFT-(M06HF) method show good agreement with the experimental values; the mean deviations of the bond lengths were 0.017 and 0.023 Å for the *EE*-DMTB and *ZZ*-DMTB isomers, respectively. The geometry optimizations were also performed with the other methods and basis sets, as summarized in the Supporting Information. The comparison with the experimental values shows that the DFT(M06HF)/D95(d) calculation is reliable for the geometric parameters, and therefore, the equilibrium geometries obtained by the DFT/TDDFT(M06HF) with D95(d) were used to calculate the absorption/emission spectra for

**Table 1.** Calculated Equilibrium Structures in the Ground ( $S_0$ ) and First Excited ( $S_1$ ) States of EE-, EZ-, and ZZ-DMTB by the DFT/TDDFT(M06HF)/D95(d) Method Compared with the X-ray Structure

geometrical parameters	EE-DMTB		EZ-DMTB		ZZ-DMTB	
	$S_0$		$S_1$		$S_0$	
	theory	expt <sup>a</sup>	theory	expt <sup>a</sup>	theory	expt <sup>a</sup>
Bond Length (Å)						
C1–C2	1.367	1.357	1.376	1.369	1.401	1.369
C2–C3	1.435	1.486	1.420	1.433	1.397	1.433
C3–C4	1.373	1.372	1.392	1.374	1.416	1.373
C4–C5	1.470	1.461	1.434	1.478	1.399	1.479
C5–C6	1.341	1.305	1.382	1.341	1.424	1.340
C6–C7	1.479	1.471	1.420	1.487	1.405	1.488
C7–C8	1.400	1.392	1.430	1.397	1.436	1.398
C8–C9	1.394	1.390	1.376	1.395	1.394	1.395
C9–C10	1.407	1.388	1.443	1.405	1.402	1.401
C10–C11	1.479	1.471	1.420	1.481	1.459	1.488
C11–C12	1.341	1.305	1.382	1.340	1.350	1.340
C12–C13	1.470	1.461	1.434	1.471	1.464	1.479
C13–C14	1.373	1.372	1.392	1.372	1.376	1.373
C14–C15	1.435	1.486	1.420	1.434	1.433	1.433
C15–C16	1.367	1.357	1.376	1.367	1.368	1.369
mean deviation	0.017				0.023	
BLA	0.101	0.128	0.041	0.104	0.037	0.106
Torsion Angle (degree)						
$\angle C3-C4-C5-C6$	180.0	-175.3	180.0	-164.3	-172.2	-163.2
$\angle C4-C5-C6-C7$	180.0	178.6	180.0	6.9	36.5	6.8
$\angle C5-C6-C7-C8$	0.0	-20.5	180.0	53.0	14.7	53.2
$\angle C9-C10-C11-C12$	180.0	-161.4	180.0	154.9	177.5	128.0
$\angle C10-C11-C12-C13$	180.0	-178.6	180.0	178.5	179.4	-6.9
$\angle C11-C12-C13-C14$	180.0	175.3	180.0	176.6	177.0	162.9

<sup>a</sup> X-ray crystallographic state cited from ref 51.

consistency in the present work. In the *EE*- and *ZZ*-DMTB isomers, the geometry change by the  $S_0 \rightarrow S_1$  transition occurs over the entire molecule, while the geometry change is relatively localized in the Z branch in the *EZ*- isomer. It is also noteworthy that the nonplanarity of the *EZ*- isomer exists in the Z branch in the  $S_0$  state and in the E branch in the  $S_1$  state. In the *ZZ*- isomer, torsion is relatively localized in the  $S_0$  state, while it is distributed over the entire molecule in the  $S_1$  state. The bond alternation was remarkable in the ground state, as seen in Figure 5. The excitation to the  $S_1$  state relaxes the bond alternation; the single bonds (C–C) were calculated to be contracted in the  $S_1$  state, and the double bond lengths (C=C) were found to be longer.

It is useful to evaluate the bond length changes in the conjugated or aromatic systems in terms of the bond length alternation (BLA) value.<sup>17,52–54</sup> The BLA values for the selected molecular fragment can be defined as the differences in the lengths between the single bond and double bond of non-hydrogen atoms by the following equation

$$\text{BLA} = \left( \frac{\sum d_{\text{single}}}{n_{\text{single}}} \right) - \left( \frac{\sum d_{\text{double}}}{n_{\text{double}}} \right) \quad (3)$$

where  $d_{\text{single}}$  and  $d_{\text{double}}$  denote the bond distance of the single and double bonds, respectively, with  $n_{\text{single}}$  and  $n_{\text{double}}$  being the

number of bonds on the backbone structure. The positive and negative signs of the BLA value indicate that the molecular unit has an aromatic and quinoid isomer, respectively.

The BLA values are shown in Figure 5. The BLA values of the *EE*-, *EZ*-, and *ZZ*- isomers in the  $S_0$  state are larger than those in the  $S_1$  state. The BLA values change significantly due to the electronic excitation. In the  $S_0$  state, the single bonds (C2–C3, C4–C5, C6–C7, C10–C11, C12–C13, and C14–C15) exhibit distances in the range of 1.43–1.47 Å, while the double bonds (C1=C2, C3=C4, C5=C6, C11=C12, C13=C14, and C15=C16) are in the range of 1.34–1.37 Å. In the *EE*-, *EZ*-, and *ZZ*- isomers, the BLA value decreases from 0.101, 0.104, and 0.106 Å in  $S_0$  to 0.041, 0.037, and 0.041 Å in  $S_1$ , respectively. The respective BLA differences between the  $S_0$  and  $S_1$  states are 0.060, 0.067, and 0.065 Å for the three isomers. This indicates that the geometry changes of the *ZZ*- and *EZ*-DMTB isomers are relatively larger than those of the *EE*- isomer. This is explained by the fact that the  $\pi$ -conjugation and the excitation are delocalized over the entire molecule in the *EE*-DMTB isomer. The BLA values calculated with the X-ray structure were 0.128 and 0.104 for *EE*-DMBT and *ZZ*-DMBT isomers, respectively.

These geometry changes of the bond lengths in the  $S_0$  and  $S_1$  states can be explained by the excitation character and the

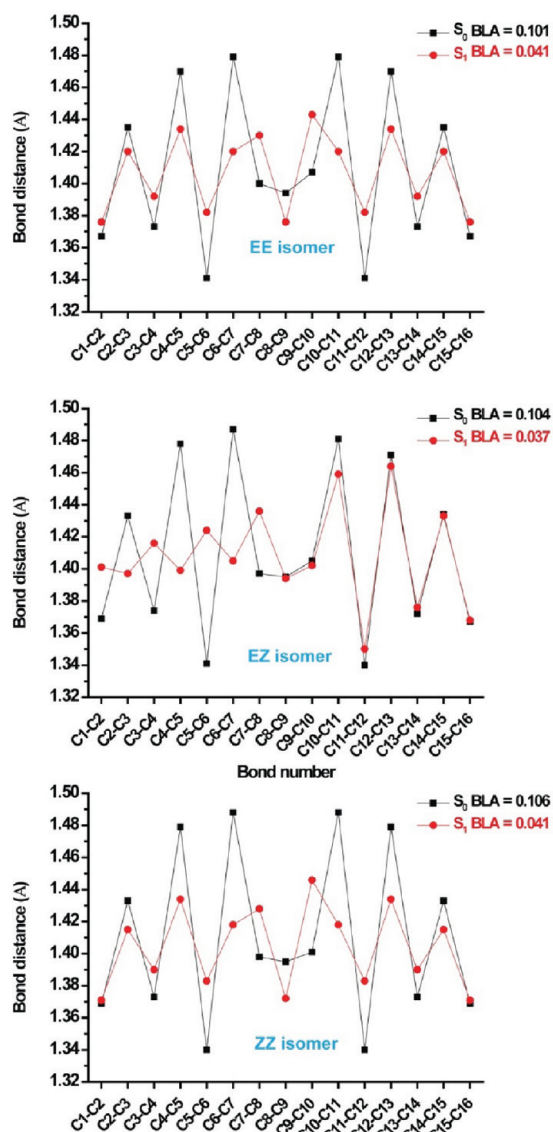


Figure 5. Bond lengths of *EE*-, *EZ*-, and *ZZ*-DMTB in the  $S_0$  and  $S_1$  states calculated at the DFT/TDDFT(M06HF)/D95(d) level of theory.

molecular orbital (MO) nodal patterns. The nodal patterns of orbitals around the highest occupied MO (HOMO) and the lowest occupied MO (LUMO) did not depend on the methods. Therefore, we can discuss the geometry changes optimized by DFT/TDDFT using the MOs employed in the SAC–CI calculations, which are shown in Figure 6 in the case of the *EE*-isomer.

The  $S_1$  state is characterized as an excitation from the HOMO ( $\pi$ ) to the LUMO ( $\pi^*$ ) in all of the considered isomers. In the HOMO, there are nodes across the C1–C2, C3–C4, C5–C6, C11–C12, C13–C14, and C15–C16 bonds, while the LUMO has bonding characters in these bonds. Thus, these bonds are contracted by the  $S_0 \rightarrow S_1$  transition. The bond lengths for the region with MO character from bonding to antibonding, on the other hand, increase upon excitation. The nodal patterns of the HOMO and LUMO in the *EZ*- and *ZZ*-isomers are similar to those of the *EE*-isomer, and the resulting bond length changes in the *EZ*- and *ZZ*-isomers caused by the  $S_0 \rightarrow S_1$  transition can be explained in a similar manner.

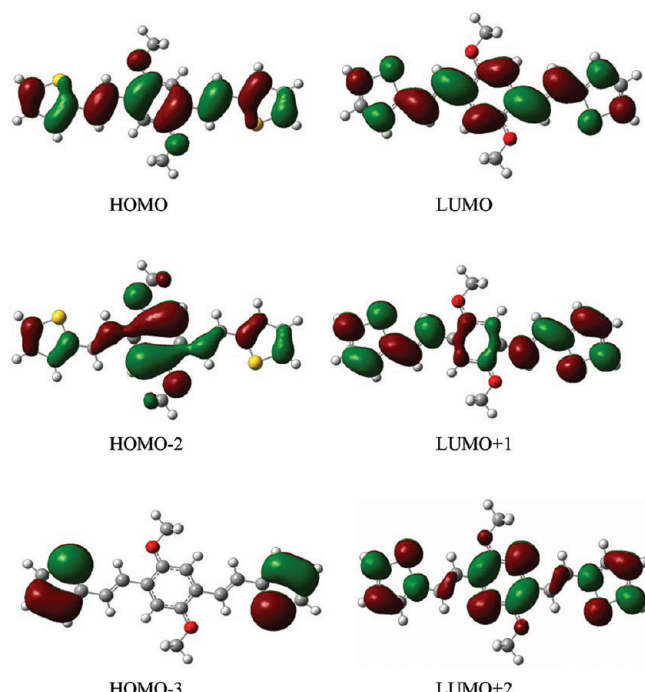


Figure 6. MOs relevant to the low-lying excited states of *EE*-DMTB.

**3.2.2. Absorption Spectrum of *EE*-DMTB.** We have computed the vertical excitation energies of the  $S_0 \rightarrow S_n$  transition of the *EE*-DMTB molecule in the gas phase and chloroform solution. The results of the low-lying, electric dipole-allowed excited states obtained by TDDFT with different functionals, M06HF, B3LYP, PBE0, and CAM-B3LYP, are presented in Table 2 with the observed values. The vertical excitation energies in chloroform solution were evaluated within the PCM. In the PCM, the nonequilibrium LR and SS calculations were performed. For the SS scheme, the SCRF iterative calculations were carried out for each excited state in PCM, while the LR calculations can obtain all excited states by single diagonalization. The transition characters as well as the excitation energies calculated by the direct SAC–CI method are given in Table 3. In the SAC–CI results, the solvent effect was taken from TDDFT with CAM-B3LYP.

First, we discuss the experimental absorption spectrum of *EE*-DMTB, which was synthesized in the present work, and its absorption/emission spectra observed in chloroform solution. The *EE*-isomer is thermally stable, and the isomerization to *EZ*- and *ZZ*- stereoisomers does not occur at room temperature, as shown later. The absorption spectrum of *EE*-DMTB measured in chloroform shows a strong absorption centered at 416 nm (2.98 eV) and two intense peaks at 355 and  $\sim$ 210 nm (3.49 and 5.90 eV) with a shoulder at 262 nm (4.73 eV); the observed spectrum is in accordance with the previous study.<sup>5</sup> The calculated spectra by TDDFT and SAC–CI methods in the gas phase, PCM with the LR scheme, and PCM with the SS scheme are compared with the observed spectrum in Figure 7.

Let us focus on the first peak observed at 2.98 eV. The calculated transition energy is in the sequence of M06HF > CAM-B3LYP > PBE0 > B3LYP; this trend is partially related to the amount of the Hartree–Fock exchange included in the applied functionals, B3LYP (20%), PBE0 (25%) and CAM-B3LYP (from 19% at short range to 65% at long range), and

**Table 2.** Excitation Energies ( $E_{\text{ex}}$ ), Absorption Wavelengths ( $\lambda_{\text{abs}}$ ), and Oscillator Strength ( $f$ ) for Low-Lying Excited States in the Gas Phase and Solvent (Chloroform) of EE-DMTB using TDDFT with M06HF, B3LYP, PBE0, and CAM-B3LYP Functionals

state	M06HF		B3LYP		PBE0		CAM-B3LYP		expt	
	$E_{\text{ex}}$ (eV)	$f$	$E_{\text{ex}}$ (eV)	$\lambda_{\text{abs}}$ (nm)						
Gas Phase										
1B <sub>u</sub>	3.67	1.503	2.90	1.315	3.00	1.358	3.30	1.426		
2B <sub>u</sub>	4.72	0.124	3.60	0.239	3.74	0.249	4.19	0.232		
3B <sub>u</sub>	5.48	0.164	4.44	0.017	4.64	0.026	5.27	0.108		
4B <sub>u</sub>	5.75	0.083	4.51	0.014	4.71	0.016	5.30	0.034		
5B <sub>u</sub>	5.96	0.259	4.71	0.132	4.96	0.118	5.42	0.082		
In Chloroform (PCM with LR) <sup>a</sup>										
1B <sub>u</sub>	3.56	1.671	2.77	1.480	2.87	1.524	3.18	1.589		
2B <sub>u</sub>	4.67	0.135	3.54	0.252	3.68	0.264	4.13	0.243		
3B <sub>u</sub>	5.43	0.217	4.44	0.019	4.64	0.032	5.25	0.111		
4B <sub>u</sub>	5.69	0.103	4.52	0.021	4.70	0.023	5.27	0.087		
5B <sub>u</sub>	5.90	0.338	4.70	0.136	4.94	0.128	5.37	0.096		
In Chloroform (PCM with SS) <sup>a</sup>										
1B <sub>u</sub>	3.49	1.771	2.69	1.597	2.79	1.641	3.10	1.696	2.98	416
2B <sub>u</sub>	4.64	0.142	3.52	0.241	3.66	0.255	4.10	0.241	3.49	355
3B <sub>u</sub>	5.38	0.275	4.44	0.027	4.64	0.046	5.22	0.090	4.73	262
4B <sub>u</sub>	5.63	0.128	4.50	0.026	4.69	0.027	5.24	0.170		
5B <sub>u</sub>	5.84	0.405	4.69	0.141	4.93	0.138	5.33	0.110	5.90	~210

<sup>a</sup> In the PCM-SS scheme, the individual SCRF calculations were performed for each excited state, while all excited states were calculated by a single calculation in the PCM-LR scheme.

**Table 3.** Excitation Energies ( $E_{\text{ex}}$ ) and Oscillator Strength ( $f$ ) for Low-Lying Excited States in the Gas Phase and in Solution (Chloroform) of EE-DMTB Calculated by the Direct SAC–CI Method

state	direct SAC–CI						expt	
	gas phase		in chloroform <sup>a</sup>				$E_{\text{ex}}$ (eV)	$\lambda_{\text{abs}}$ (nm)
	$E_{\text{ex}}$ (eV)	$f$	$E_{\text{ex}}$ (eV)	$f$	transition character			
1B <sub>u</sub>	3.21	1.143	3.01	1.318	H → L(85%)		2.98	416
2B <sub>u</sub>	3.97	0.369	3.88	0.375	H–2 → L (56%), H → L+1 (25%)		3.49	355
3B <sub>u</sub>	5.17	0.165	5.12	0.298	H → L+2 (60%), H–2 → L (26%)		4.73	262
4B <sub>u</sub>	5.49	0.262	5.43	0.243	H–3 → L (56%), H–4 → L+1 (29%)			
5B <sub>u</sub>	5.85	0.145	5.74	0.165	H → L+3 (30%), H–1 → L+1 (29%)		5.90	~210

<sup>a</sup> The solvent effect is calculated with TDDFT(CAM-B3LYP) PCM-SS.

M06HF (100%). To avoid such arbitrariness, we performed the SAC–CI calculation. The TD-B3LYP value of 2.90 eV in the gas phase is in good agreement with the observed value, however, including the solvent effect of 0.21 eV in chloroform solution; the theoretical transition energy results in 2.69 eV, which deviates by ~0.3 eV from the experimental value of 2.98 eV. The TD-CAM-B3LYP (PCM-SS) in chloroform solution, on the other hand, shows good agreement with the experiment; the deviation is 0.12 eV. The TD-PBE0 (PCM-SS) provides a deviation as large as 0.19 eV. The TD-M06HF gives a rather high excitation energy by ~0.5 eV compared with the experimental value.

Next, we discuss the two higher peaks observed at 3.49 and ~5.90 eV with a shoulder at 4.73 eV. The solvent effect in the second peak at 3.49 eV was evaluated to be smaller than the first excited state at 0.08–0.09 eV by the TDDFT (PCM-SS) calculations. The TDDFT calculations tend to overestimate

the transition energies of the second peak, namely, 4.64, 3.52, 3.66, and 4.10 eV compared to the experimental value of 3.49 eV. For the higher shoulder observed at 4.73 eV, TDDFT (PCM-SS) calculated the transitions at 5.38 eV with M06HF, 4.69 eV with B3LYP, 4.93 eV with PBE0, and 5.22, 5.24, and 5.33 eV with CAM-B3LYP from the viewpoint of the calculated oscillator strength but with different transition character. These transition energies were calculated with the PCM-SS scheme, and the solvent effect was calculated for each excited state. Thus, for the peaks higher than the  $S_0 \rightarrow S_1$  transition, the theoretical calculations tend to overestimate the excitation energies compared to the experimental values.

Because the assignment of the higher peaks is difficult with TDDFT calculations, as seen above, the SAC–CI result in Table 3 is useful for the assignment. The SAC–CI

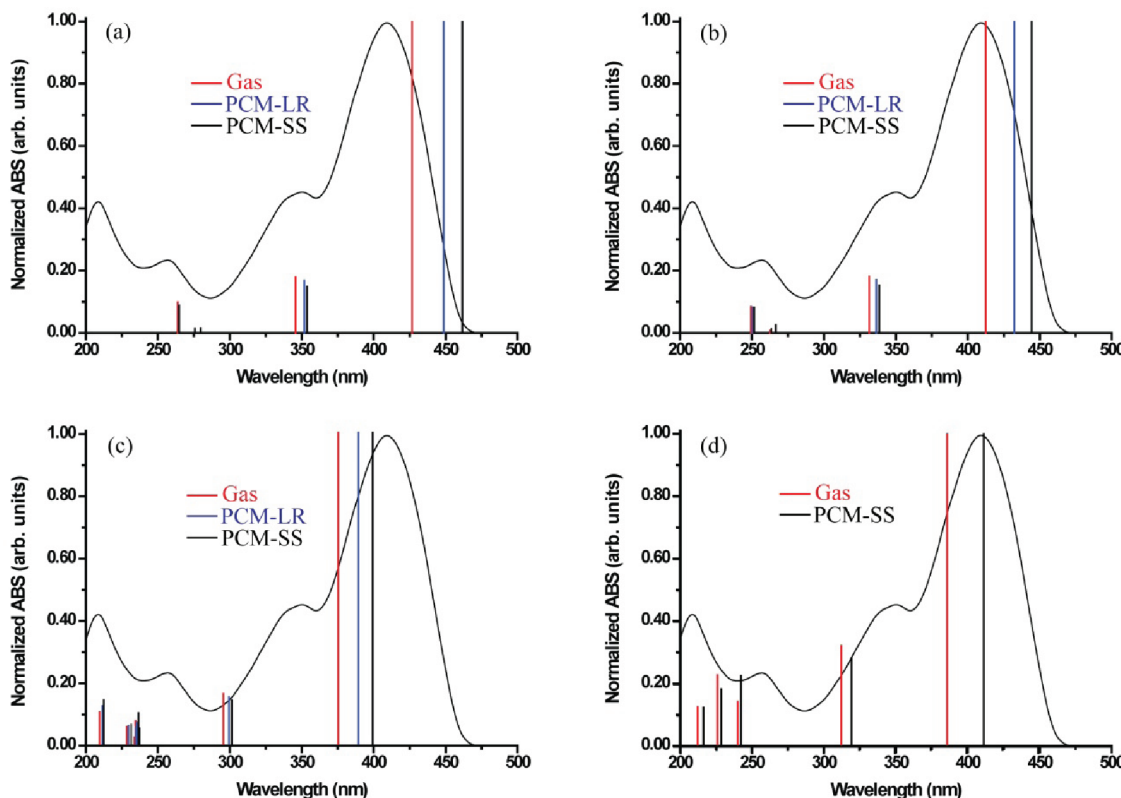


**Figure 7.** Experimental absorption spectrum of EE-DMTB observed in chloroform solution and theoretical spectra (vertical solid lines) calculated using (a) B3LYP, (b) PBE0 (c) CAM-B3LYP, and (d) direct SAC-CI. Theoretical spectra are shown for the gas phase (Gas) and in chloroform (PCM-SS/LR). The direct SAC-CI spectrum in chloroform is calculated with the correction using CAM-B3LYP (PCM-SS).

assignments of the lower peaks are identical to those of TDDFT, while they are different for the higher peaks. The first peak at 2.98 eV was assigned to the transition from the HOMO to LUMO ( $1B_u$ ), abbreviated as  $H \rightarrow L$  in the present paper, and the second peak ( $2B_u$ ) at 3.49 eV was attributed to the linear combination of the  $H-2 \rightarrow L$  and  $H \rightarrow L+1$  components. The shoulder at 4.73 eV was assigned to the  $3B_u$  state characterized as  $H \rightarrow L+2$ . The higher peak observed at  $\sim 5.90$  eV was attributed to the  $4B_u$  and  $5B_u$  states characterized as  $H-3 \rightarrow L$  and  $H \rightarrow L+3$ , respectively. All of these states are assigned to the  $\pi \rightarrow \pi^*$  transition. The relevant MOs for these transitions are shown in Figure 6. Note that we use the MOs, and the Kohn-Sham orbitals concerned in the excitations are similar to MOs. The HOMO and LUMO are delocalized over the entire region of molecule, while other MOs are relatively localized in some region; the  $H-2$  and  $L+2$  orbitals are localized in the central benzene unit, and the  $H-3$  and  $L+1$  orbitals are localized in the thiophene units.

The PCM-SAC-CI method has recently been developed;<sup>37,38</sup> however, a scheme for calculating large systems has not been established, and therefore, we calculated the spectrum with the correction of the solvent effect using TDDFT calculations. In this study, the solvent correction for the  $i \rightarrow a$  transition was estimated from the CAM-B3LYP calculations as

$$\Delta\Delta E_{i \rightarrow a, (\text{solv})} = \Delta E_{i \rightarrow a, (\text{solv})}^{\text{CAM-B3LYP}} - \Delta E_{i \rightarrow a, (\text{vac})}^{\text{CAM-B3LYP}} \quad (4)$$

where  $\Delta E_{i \rightarrow a, (\text{vac})}^{\text{CAM-B3LYP}}$  and  $\Delta E_{i \rightarrow a, (\text{solv})}^{\text{CAM-B3LYP}}$  are the CAM-B3LYP transition energies in vacuum and in solution, respectively. The oscillator strength in x circumstance ( $x = \text{solv}$  or  $\text{vac}$ ) may be written as

$$f_{i \rightarrow a, (x)} = \frac{2}{3} \Delta E_{i \rightarrow a, (x)} T_{i \rightarrow a, (x)} \quad (5)$$

where  $T = \mathbf{m}_{ia} \cdot \mathbf{m}_{ai}$  and  $\mathbf{m}_{ia}$  is the transition dipole moment in the length form. The solvent shift of oscillator strengths are written as

$$\Delta f_{i \rightarrow a, (\text{solv})} = f_{i \rightarrow a, (\text{solv})} - f_{i \rightarrow a, (\text{vac})} \quad (6)$$

Using eqs 4 and 5, we obtain

$$\begin{aligned} \Delta f_{i \rightarrow a, (\text{solv})} &= \frac{2}{3} (\Delta E_{i \rightarrow a, (\text{vac})} \Delta T_{i \rightarrow a, (\text{solv})} \\ &\quad + \Delta \Delta E_{i \rightarrow a, (\text{solv})} T_{i \rightarrow a, (\text{solv})}) \end{aligned} \quad (7)$$

with  $\Delta T_{i \rightarrow a, (\text{solv})} = T_{i \rightarrow a, (\text{solv})} - T_{i \rightarrow a, (\text{vac})}$ . The first term in eq 7 represents the solvent effect on the transition density, and the second one is the contribution from the transition energy shift. In this study, we neglected the second contribution that was about a few percent or less for the total oscillator strength of this molecule. Consequently, the SAC-CI transition energies and oscillator strengths with solvent correction are given by

$$\Delta E_{i \rightarrow a, (\text{solv})}^{\text{SAC-CI}} = \Delta E_{i \rightarrow a, (\text{vac})}^{\text{SAC-CI}} + \Delta \Delta E_{i \rightarrow a, (\text{vac})}^{\text{CAM-B3LYP}} \quad (8)$$

**Table 4.** Mulliken Charges in the Fragment of EE-DMTB Calculated by the Direct SAC-CI/D95(d)

state	Mulliken charge		
	I <sup>a</sup>	II <sup>a</sup>	III <sup>a</sup>
S <sub>0</sub> State Geometry <sup>b</sup>			
XA <sub>g</sub>	0.007	-0.106	0.198
1B <sub>u</sub>	-0.012	-0.118	0.261
2B <sub>u</sub>	-0.004	-0.135	0.278
3B <sub>u</sub>	0.024	-0.087	0.126
4B <sub>u</sub>	0.118	-0.175	0.112
5B <sub>u</sub>	-0.024	-0.067	0.180
S <sub>1</sub> State Geometry <sup>b</sup>			
XA <sub>g</sub>	0.020	-0.134	0.227
1B <sub>u</sub>	0.001	-0.140	0.279
2B <sub>u</sub>	-0.020	-0.188	0.417

<sup>a</sup> Regions I, II, and III correspond to the unit of thiophene, vinylene, and benzene with two methoxy groups, respectively. <sup>b</sup> S<sub>0</sub> and S<sub>1</sub> geometries are optimized by the DFT/TDDFT(M06HF) method.

and

$$f_{i \rightarrow a, (\text{solv})}^{\text{SAC-CI}} = f_{i \rightarrow a, (\text{vac})}^{\text{SAC-CI}} + \frac{\Delta E_{i \rightarrow a, (\text{vac})}^{\text{SAC-CI}}}{\Delta E_{i \rightarrow a, (\text{vac})}^{\text{CAM-B3LYP}}} \Delta f_{i \rightarrow a, (\text{solv})}^{\text{CAM-B3LYP}} \quad (9)$$

On the basis of the transition character, we can correlate the excited states between TDDFT (CAM-B3LYP) and SAC-CI, and therefore, we incorporate the solvation effect of the TDDFT (CAM-B3LYP) into SAC-CI. The corrected SAC-CI excitation energies are also given in Table 3; they were 3.01, 3.88, 5.12, 5.43, and 5.74 eV for the five low-lying excited states that showed reasonable agreement with the experimental values of 2.98, 3.49, 4.73, and 5.90 eV, except for the second peak. The solvent effect on the oscillator strength is not negligible in the TDDFT results. The corrected oscillator strength is also given in Table 3. Consequently, the SAC-CI spectrum shows good agreement with the experimental one, as compared in Figure 7d; for example, the SAC-CI spectrum shows better agreement with the experiment in the high-energy region, and the intensity ratio between the first and second peaks is better in SAC-CI. This suggests that the present procedure is acceptable for the estimation of the excitation energies in solution and therefore is used for the calculations for other EZ- and ZZ- isomers in the next subsection.

The energy shift in transition energies by the solvent effect is analyzed using the Mulliken charges in the ground and excited states. The reorganization of the Mulliken charges in the excited states of EE-DMTB is examined with the three fragments of the molecule, namely, thiophene (region I), vinylene (region II), and benzene with two methoxy groups units (region III). The charges in these regions calculated by the SAC-CI method are presented in Table 4. Because EE-DMTB has a symmetric structure, the molecule has no dipole moment. However, the charge polarization changes due to excitation and the difference of the charge polarization between the ground and excited states affect the excitation energies. The charges of the regions II and III are negative and positive, respectively, in both the ground and excited states. The charge reorganization is large in regions II and III.

Because the 2B<sub>u</sub> state is assigned to H-2 → L, electron density reorganizes from region III to regions I and II, which can be seen in the Mulliken charge. The 3B<sub>u</sub> and 4B<sub>u</sub> states, on the other hand, are H → L+2 and H-3 → L, and therefore, the electron density reorganizes into central region III. In the 4B<sub>u</sub> state, the charge reorganization in region I is characteristic because the H-3 orbital is localized in region I. The charge separation in the 1B<sub>w</sub>, 2B<sub>w</sub> and 5B<sub>u</sub> states is slightly larger than that in the ground state, and the charge distributions are different from those of the ground state. Region I is negative in the 1B<sub>w</sub>, 2B<sub>w</sub> and 5B<sub>u</sub> states, whereas it has small positive charge in the ground state. Therefore, the equilibrium orientation of the polar solvent is expected to be different between the ground state and the 1B<sub>w</sub>, 2B<sub>w</sub> and 5B<sub>u</sub> states. Although the dipole moment of the EE-DMTB is zero, the solvent effect on the transition energy is not so trivial at 0.05–0.20 eV because the electron density distribution is different in each state.

**3.2.3. Absorption Spectra of EZ- and ZZ-DMTB.** The absorption spectra of the EZ- and ZZ-DMTB isomers have also been investigated, which concerns the structure and  $\pi$ -conjugation-length dependence on the excited states. The absorption spectra of these isomers were calculated by the direct SAC-CI method with the TD-CAM-B3LYP (PCM-SS) correction. The results are summarized in Table 5 with the experimental values extracted from the UV-vis spectra observed in the previous work.<sup>5</sup> In Figure 8, theoretical spectra are compared with the UV-vis spectra<sup>5</sup> in the range of 200–500 nm. We also observed the transient absorption spectra contributed from EZ- and ZZ-isomers; however, the decomposition of the spectra into each isomer is not possible so that we compared our theoretical spectra with the previous ones.<sup>5</sup> As can be seen in Figure 8, the direct SAC-CI calculations reproduced the experimental spectra in both peak positions and absorption intensity satisfactorily compared to the characteristics of the EE- isomer; the absorption peaks of the EZ- and ZZ-DMTB isomers shift to the higher-energy region compared to those of the EE- isomer, which reflects the shorter effective  $\pi$ -conjugation length of the two isomers, with the absorption intensity in the low-energy region decreasing.

Let us first discuss the absorption spectrum of the EZ-DMTB isomer. The lowest excited state observed at 377 nm (3.29 eV) is assigned to the H → L transition (1A) calculated at 3.38 eV. The solvent effect in this state was calculated to be -0.18 eV. The second peak centered at 310 nm (4.00 eV) is assigned to the 2A (H-1 → L) and 3A (H-2 → L) states calculated at 3.99 and 4.40 eV, respectively. The third peak observed at ~250 nm (4.96 eV) is assigned to the 4A and 5A states calculated at 4.63 and 4.85 eV, respectively, although the calculated oscillator strengths of these transitions are too small for this peak. In the EZ- isomer, the H-1 → L transition is stabilized compared to that in the EE- isomer. The difference of the absorption intensity between the EE- and EZ- isomers was also properly reproduced. The oscillator strength of the first peak in the EZ- isomer is reduced compared to that of other higher peaks, namely, the oscillator strength of the EZ- isomer is  $f = 0.568$ , while that of the EE- isomer is  $f = 1.143$ .

The spectrum of the ZZ- isomer is very characteristic; the absorption intensity in the high-energy region is comparative and even larger than that of the first peak. The first peak observed at ~345 nm (3.60 eV) is also attributed to the H → L transition calculated at 3.52 eV by the SAC-CI method; the solvent effect correction was calculated to be -0.16 eV. The oscillator strength

**Table 5.** Excitation Energies ( $E_{\text{ex}}$ ), Absorption Wavelengths ( $\lambda_{\text{abs}}$ ), and Oscillator Strength ( $f$ ) for Low-Lying Excited States in a Solvent (Chloroform) of EZ- and ZZ-DMTB Calculated by the Direct SAC-CI/D95(d) with the Solvent Effect

state	direct SAC-CI with solvent effect <sup>a</sup>				expt <sup>b</sup>	
	$E_{\text{ex}}$ (eV)	$\lambda_{\text{abs}}$ (nm)	$f$	transition character	$E_{\text{ex}}$ (eV)	$\lambda_{\text{abs}}$ (nm)
EZ-DMTB						
1A	3.38	367	0.568	H → L (85%)	3.29	377
2A	3.99	311	0.237	H-1 → L (47%), H → L+1 (28%)	4.00	310
3A	4.40	282	0.152	H-2 → L (61%), H → L+1 (14%)		
4A	4.63	268	0.053	H-1 → L+1 (23%), H-3 → L (18%), H → L+3 (17%), H-2 → L+2 (14%)		
5A	4.85	256	0.053	H-3 → L+1 (21%), H-3 → L (17%), H → L+1 (12%), H-2 → L+1 (12%)	4.96	250
ZZ-DMTB						
1A <sub>u</sub>	3.52	352	0.229	H → L (81%), H-2 → L+1 (16%)	3.60	345
2A <sub>u</sub>	4.03	308	0.171	H-1 → L (66%)	4.28	290
3A <sub>u</sub>	5.03	246	0.019	H-2 → L (50%), H → L+1 (35%)		
4A <sub>u</sub>	5.18	240	0.138	H-3 → L (27%), H-2 → L+1 (21%), H → L+3 (16%), H-1 → L+2 (13%)	5.04	246
5A <sub>u</sub>	5.57	223	0.104	H-4 → L (40%), H-3 → L+1 (24%)	6.20	~200

<sup>a</sup> The solvent effect is calculated with TDDFT(CAM-B3LYP) PCM-SS. <sup>b</sup> Cited from ref 5.

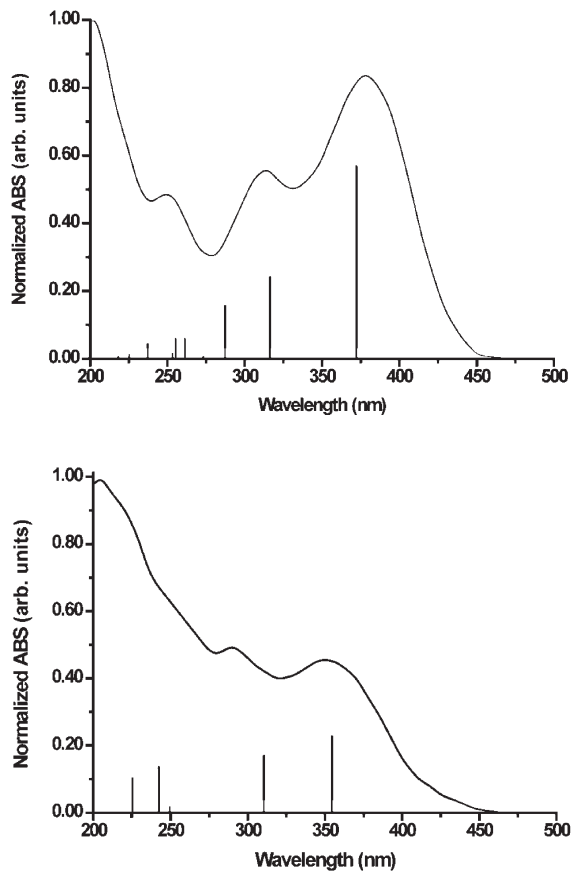


**Figure 8.** Absorption spectra of EZ-DMTB (upper panel) and ZZ-DMTB (lower panel) isomers observed in acetonitrile solution cited from ref 5 and theoretical spectra (solid vertical lines) calculated by direct SAC-CI/D95(d) with the solvent effect correction using TDDFT(CAM-B3LYP).

of this transition was computed as  $f = 0.229$ , which is much smaller than those of the EE- and EZ- isomers. The second peak centered at  $\sim 290$  nm (4.28 eV) in the UV-vis spectrum was assigned to the H-1 → L transition calculated at 4.03 eV. The strong absorption was observed at  $\sim 200$  nm (6.20 eV) with the shoulder at 246 nm (5.03 eV). For these peaks, the 4B<sub>u</sub> and 5B<sub>u</sub> states whose transitions are characterized as H-3 → L and H-4 → L, respectively, calculated at 5.18 and 5.57 eV were credited. As in the EZ- isomer, the H-1 → L transition is stabilized, and the H → L+2 transition is destabilized in comparison with those in the EE- isomer.

**3.2.4. Emission Spectra of EE-, EZ-, and ZZ-DMTB.** Fluorescence spectra of three isomers have been studied by TDDFT (PCM-SS) and direct SAC-CI calculations. The fluorescence energies were calculated by the vertical  $S_0 \rightarrow S_1$  transition at the equilibrium geometry of the  $S_1$  state optimized by the TDDFT-(M06HF)/D95(d) method. Table 6 summarizes the TDDFT and SAC-CI results with the experimental value of EE- and ZZ-DMTB. The observed fluorescence spectrum of EE-DMTB is shown in Figure 2, and the transient fluorescence spectra contributed from the EE-, EZ-, and ZZ- isomers are displayed in Figure 3.

Let us first discuss the fluorescence spectrum of the EE- isomer. The strong fluorescence has been observed with the peak maximum at 458 nm (2.71 eV) and the shoulder at 481 nm (2.58 eV), as seen in Figure 2. The TDDFT and SAC-CI calculations provided almost similar emission energies in the range of 2.48–2.71 eV, which can be compared to the experimental value of 2.71 eV. The TDDFT calculations with the B3LYP and PBE0 functionals provided slightly lower energies of 2.48 and 2.55 eV, respectively, while the calculation with the CAM-B3LYP functional gave an excellent value of 2.73 eV. The SAC-CI method calculated a value of 2.64 eV at the gas-phase geometry for this emission. We also performed the geometry optimization in chloroform by the TDDFT (PCM-SS) method.

**Table 6.** Fluorescence Energies ( $E_{\text{em}}$ ), Wavelengths ( $\lambda_{\text{em}}$ ), and Oscillator Strength ( $f$ ) of EE-, EZ-, and ZZ-DMTB Calculated by TDDFT (PCM-SS) and Direct SAC-CI with Solvent Effects

method	$E_{\text{em}}$ (eV)	$\lambda_{\text{em}}$ (nm)	$f$	transition character
EE-Isomer				
M06HF	2.98	415	1.568	H → L (91%)
B3LYP	2.48	499	1.554	H → L (100%)
PBE0	2.55	487	1.590	H → L (100%)
CAM-B3LYP	2.73	455	1.586	H → L (95%)
SAC-CI (gas) <sup>a</sup>	2.64	469	1.193	H → L (87%)
SAC-CI (sol) <sup>b</sup>	2.71	458	1.490	H → L (97%)
expt	2.71	458	—	
EZ-Isomer				
M06HF	2.16	574	0.284	H → L (86%)
B3LYP	1.90	654	0.358	H → L (96%)
PBE0	1.94	640	0.363	H → L (96%)
CAM-B3LYP	2.06	601	0.356	H → L (91%)
SAC-CI (gas) <sup>a</sup>	2.30	540	0.247	H → L (93%)
SAC-CI (sol) <sup>b</sup>	2.34	531	0.357	H → L (94%)
expt	—	—	—	
ZZ-Isomer				
M06HF	3.10	400	0.952	H → L (91%)
B3LYP	2.53	491	0.870	H → L (100%)
PBE0	2.60	478	0.897	H → L (100%)
CAM-B3LYP	2.82	440	0.948	H → L (95%)
SAC-CI (gas) <sup>a</sup>	2.90	428	0.660	H → L (98%)
SAC-CI (sol) <sup>b</sup>	2.62	473	0.773	H → L (98%)
expt	2.68	463	—	

<sup>a</sup>Calculated at the TDDFT(M06HF) geometry in the gas phase.

<sup>b</sup>Calculated at the TDDFT(M06HF, PCM-SS) geometry in chloroform solution.

The SAC-CI calculation with the optimized geometry in chloroform gave the emission energy of 2.71 eV, in excellent agreement with the experimental value. This implies that the geometry optimization in the solution is also one of the important issues in the calculation of the emission energy. The oscillator strength of this transition is large, on the order of  $f = 1.2\text{--}1.6$  depending on the computational method, which indicates the strong emission of the *EE*-isomer. Actually, for this *EE*-isomer, strong fluorescence has been observed in the present work, even though we have to consider other quenching processes for precise estimation. The transition character is described as  $L \rightarrow H$ , whose configuration is localized compared to the absorption.

For considering the solvent effect on fluorescence, we examined the charge distribution in the  $S_0$  and  $S_1$  states at the  $S_1$  state geometry. The reorganization of the charges in the  $S_0$  and  $S_1$  states of the *EE*-DMTB is given in Table 4. The charge reorganization at the  $S_1$  state geometry is not similar to the reorganization at the  $S_0$  state geometry. At the  $S_1$  state geometry, the total Mulliken charges in regions I and III are positive in both  $X\text{A}_g$  and  $1\text{B}_u$  states, and the charge in region II is negative. It implies that the solvatochromic shift in the emission in the polar solvent is small because the absolute effect is canceled out in the

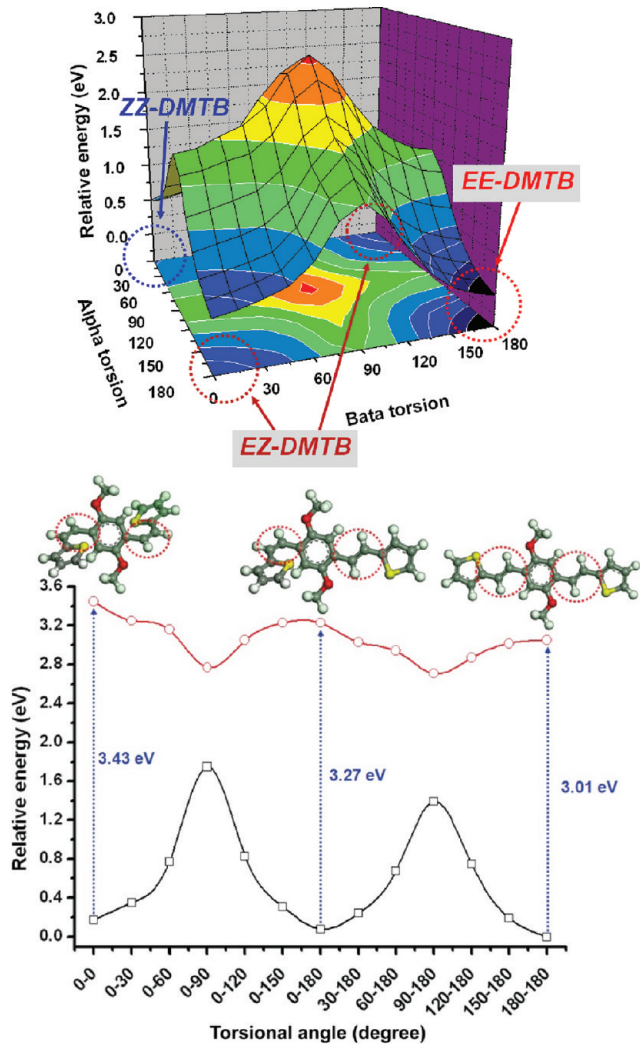


**Figure 9.** Potential energy surface (left) of the ground state and potential energy curves (right) of the  $S_0$  and  $S_1$  states of DMTB for isomerization calculated by DFT/TDDFT(M06HF).

$S_0$  and  $S_1$  states. This is confirmed by the calculated fluorescence energy in the gas phase and in solution.

The fluorescence energies of the *EZ*- and *ZZ*- stereoisomers were also calculated by both the TDDFT and SAC-CI methods. The dependence of the computational methods or functionals on the emission energies of these stereoisomers is almost the same as that of the *EE*-isomer. The SAC-CI method with the optimized structure in solution predicted the emission energies of 2.34 and 2.68 eV for *EZ*- and *ZZ*-isomers, respectively, whose relative energies are of interest; the emission energy of the *EZ*-isomer is lower than that of the *ZZ*-isomer. This difference of emission energies originates in the molecular structure as the trend is also obtained by the TDDFT calculations. The transient spectra in Figure 3 indicate that the isomerization to the *EZ*- and *ZZ*-isomers occurs. The oscillator strengths of these isomers were calculated as  $f = 0.357$  and  $0.773$  for the *EZ*- and *ZZ*-isomers, respectively. This trend of intensity changes between the isomers is consistent with the experimental findings in Figure 3b, in which decay of the fluorescence was observed probably caused by the isomerization. The weak emission intensities of these isomers are similar to those of the absorption,

but the character of the  $S_1$  state is localized as  $L \rightarrow H$  as in the *EE*-isomer.

**3.2.5. Isomerization among the Three Stereoisomers.** Waszkiewicz and co-workers<sup>5</sup> investigated how the electrochemical process may cause isomerization of these compounds. In the present work, the isomerization among three isomers, *EE*-, *EZ*-, and *ZZ*-DMBT isomers, has been examined in both the  $S_0$  and  $S_1$  potential energy surfaces (PESs) using the DFT/TDDFT-(M06HF) method. In particular, the photoisomerization is of interest because the transient absorption/fluorescence spectra apparently indicate the photoisomerization. The isomerization among these isomers occurs at the vinylene double bonds, and therefore, the PESs were calculated by the partial optimization with the torsion angle being fixed and relaxing all other degrees of freedom. The torsion angle ( $\theta$ ) is defined as an angle between the planes formed by the vinylene linkages units. The torsion angles of  $\theta_1 = \angle C_4-C_5-C_6-C_7$  and  $\theta_2 = \angle C_{10}-C_{11}-C_{12}-C_{13}$  (in Figure 1) in the *Z*- and *E*-isomers are defined as  $\theta = 0$  and  $180^\circ$ , respectively. Structures at various torsional angles (from  $\theta = 0$  to  $180^\circ$  in steps of  $30^\circ$ ) were partially optimized by DFT/TDDFT(M06HF)/D95(d) for the  $S_0$  and  $S_1$  states.

A two-dimensional PES of the  $S_0$  state is presented in the left panel of Figure 9. The PES shows that three local minima exist for the *EE*- ( $\theta_1 = 180^\circ$  and  $\theta_2 = 180^\circ$ ), *EZ*- ( $\theta_1 = 180^\circ$  and  $\theta_2 = 0^\circ$ ), and *ZZ*- isomers ( $\theta_1 = 0^\circ$  and  $\theta_2 = 0^\circ$ ). The PES also shows that the *EE*-DMBT isomer ( $\theta_1 = 180^\circ$  and  $\theta_2 = 180^\circ$ ) is more stable in a planar configuration by  $\sim 0.2$  eV than the *EZ*- and *ZZ*-DMBT isomers. An explanation is the strong  $\pi$ -conjugation and the intramolecular C–H···O hydrogen bond interaction that induces the geometry stabilization. At the torsional angle of  $90^\circ$ , the energy barrier for the perpendicular conformation of the *EE*-, *EZ*-, and *ZZ*- isomers amounts to  $\sim 1.5$  eV. It is indicated that all of the isomers can be distinguishable, and thermal isomerization between the three isomers does not occur.

The photoisomerization for  $ZZ \rightarrow EZ \rightarrow EE$  and  $EZ \rightarrow EE$  was observed in ref 5. The transient spectra are also observed in the present work. The partial optimization of the  $S_0$  and  $S_1$  states was performed, and their potential energy curves along the torsion angle are shown in the right panel of Figure 9. The PES of the  $S_1$  state shows that the Franck–Condon region of the  $S_1$  state corresponds to the transition state in the  $S_0$  state, and the geometries at around  $\theta_1 = 90^\circ$  and  $\theta_2 = 90^\circ$  are stable. Therefore, after the  $S_0 \rightarrow S_1$  transition, each isomer relaxes to the geometric region of  $\theta_1 = 90^\circ$  or  $\theta_2 = 90^\circ$  on the  $S_1$  surface and nonradiatively decays to the  $S_0$  state. Comparing to the experimental excitation energies of 3.05, 3.30, and 3.60 eV at the ground-state geometries available for the *EE*-, *EZ*-, and *ZZ*-DMTB isomers, respectively,<sup>5,6</sup> it can be seen that the TD-M06HF (PCM-SS)/D95(d) calculation gives the excitation energies of the  $S_1$  transition, 3.01, 3.34, and 3.76 eV, for the *EE*-, *EZ*- and *ZZ*- isomers, respectively. The PES indicates that the sequential excitation of the *ZZ*- or *EZ*- isomer results in the formation of the *EE*- isomer that was monitored in ref 5, and the formation of the *ZZ*- and *EZ*- isomers occurs from the *EE*- isomer by UV irradiation, which was observed in the present transient electronic spectra.

The photophysical properties of the *EE*-, *EZ*-, and *ZZ*- isomers are different and characteristic so that their conformation is discernible with absorption/fluorescence; for example, fluorescence is strong in the *EE*- isomer and weak in the *ZZ*- isomer. The photoisomerization also occurs using the UV irradiation, as

shown in the transient UV–vis absorption and fluorescence spectra that are discussed in section 3.1. These results show that the photophysical properties of DMBT can be controlled by the conformation constraint and indicate the possibility of a photofunctional molecular device such as a switching function.

## 4. CONCLUSION

Absorption and fluorescence spectra of 1,4-dimethoxy-2,5-bis[2-(thien-2-yl)ethenyl] benzene (DMTB) have been investigated for the *EE*-, *EZ*-, and *ZZ*- isomers. The *EE*-DMTB was prepared, and its absorption/emission spectra were observed. The transient absorption/emission spectra were also observed by sequential irradiation for the *EE*-DMTB, which shows photoisomerization among the three isomers. The photophysical properties and photoisomerization of DMTB have also been theoretically studied by the direct SAC–CI and TDDFT calculations.

The characteristics of the absorption spectra of the three isomers were satisfactorily reproduced by the direct SAC–CI and TDDFT methods in both peak position and intensity. The relative stability of the three isomers and the photoisomerization among these isomers have also been examined theoretically. The  $S_0$  and  $S_1$  state geometries were calculated by the DFT/TDDFT-(M06HF) method, and the calculated  $S_0$  structures of the *EE*- and *ZZ*- isomers agree well with those of the X-ray structures. The geometry relaxation in the  $S_1$  state was interpreted with regard to the excitation character. The solvent effect in the absorption and fluorescence spectra was examined by the PCM and was found to be 0.05–0.20 eV, reflecting the charge polarization.

The present results show that the photophysical properties of DMTB can be controlled with the conformation constraint by introducing the substituents and also indicate the possibility of a photofunctional molecular device such as a switching function.

## ■ ASSOCIATED CONTENT

**S Supporting Information.** Equilibrium structure of the  $S_0$  state of *EE*-DMBT calculated by DFT(B3LYP, M06, M06HF) and MP2 with D95(d) and 6-311G(d) (Table S1), equilibrium structure of the  $S_1$  state of *EE*-DMBT calculated by CIS and TD-DFT(B3LYP, PBE0, CAM-B3LYP, M06, M06HF) with D95(d) (Table S2), basis set dependence of excitation energies for low-lying excited states in the gas phase of *EE*-DMBT by TD-DFT(B3LYP, CAM-B3LYP) (Table S3), and excitation energies, absorption wavelengths, and oscillator strengths for low-lying excited states in the gas phase and solution (chloroform) of *EZ*- and *ZZ*-DMBT using TD-DFT(CAM-B3LYP)/D95(d) (Table S4). This material is available free of charge via the Internet at <http://pubs.acs.org.org>.

## ■ AUTHOR INFORMATION

### Corresponding Author

\*Tel +66-2-5625555, ext 2227. Fax +66-2-5793955. E-mail: fsciswsm@ku.ac.th

## ■ ACKNOWLEDGMENT

We appreciate support from the Thailand Research Fund (RTA5380010 to S.H. and MRG5480273 to S.S.). S.S. was supported by the Science Research Fund (ScRF), ScAWAKE

from the Faculty of Science, Kasetsart University, Department of Chemistry, the Asea-Uninet, the University of Vienna, and the grants from the JENESYS programme, Kasetsart University Research and Development Institute (KURDI), National Nanotechnology Center (NANOTEC), Laboratory of Computational and Applied Chemistry (LCAC), the Commission on Higher Education, Ministry of Education [through the National Research University Project of Thailand (NRU) and the National Center of Excellence for Petroleum, Petrochemical and Advanced Materials (NCEPPAM)], the and Institute for Molecular Science (IMS) are gratefully acknowledged for partial support and research facilities. M.E. and R.F. acknowledge the support from JST-CREST, a Grant-in-Aid for Scientific Research from the Japanese Society for the Promotion of Science (JSPS) and the Ministry of Education, Culture, Sports, Science and Technology (MEXT), Strategic Programs for Innovative Research (SPIRE), and the Computational Materials Science Initiative (CMSI), Japan. The computations were partly performed using the Research Center for Computational Science in Okazaki, Japan.

## ■ REFERENCES

- (1) Freund, T.; Scherf, U.; Mullen, K. *Angew. Chem., Int. Ed.* **1994**, *33*, 2424.
- (2) Leuninger, J.; Trimpin, S.; Rädder, H.-J.; Müllen, K. *Macromol. Chem. Phys.* **2001**, *202*, 2832.
- (3) Blouin, N.; Michaud, A.; Wakim, S.; Boudreault, P. L. T.; Leclerc, M.; Vercelli, B.; Zecchin, S.; Zotti, G. *Macromol. Chem. Phys.* **2006**, *207*, 166.
- (4) Fukazawa, A.; Yamaguchi, S. *Chem.—Asian J.* **2009**, *4*, 1386.
- (5) Waskiewicz, K.; Gabanski, R.; Motyka, R.; Lapkowski, M.; Suwinski, J.; Zak, J. *J. Electroanal. Chem.* **2008**, *617*, 27.
- (6) Fuks-Janczarek, I.; Reshak, A. H.; Kuznik, W.; Kityk, I. V.; Gabanski, R.; Lapkowski, M.; Motyka, R.; Suwinski, J. *Spectrochim. Acta, Part A* **2009**, *72*, 394.
- (7) Runge, E.; Gross, E. K. U. *Phys. Rev. Lett.* **1984**, *52*, 997.
- (8) Stratmann, R. E.; Scuseria, G. E.; Frisch, M. J. *J. Chem. Phys.* **1998**, *109*, 8218.
- (9) Perdew, J. P.; Ruzsinsky, A.; Tao, J.; Staroverov, V. N.; Scuseria, G. E.; Csonka, G. I. *J. Chem. Phys.* **2005**, *123*, 062201.
- (10) Dreuw, A.; Head-Gordon, M. *Chem. Rev.* **2005**, *105*, 4009.
- (11) Barone, V.; Polimeno, A. *Chem. Soc. Rev.* **2007**, *36*, 1724.
- (12) Jacquemin, D.; Perpèt, E. A.; Ciofini, I.; Adamo, C. *Acc. Chem. Res.* **2009**, *42*, 326.
- (13) Suramitr, S.; Kerdcharoen, T.; Srihirin, T.; Hannongbua, S. *Synth. Met.* **2005**, *155*, 27.
- (14) Suramitr, S.; Hannongbua, S.; Wolschann, P. *J. Mol. Struct.: THEOCHEM* **2007**, *807*, 109.
- (15) Chidthong, R.; Hannongbua, S.; Aquino, A.; Wolschann, P.; Lischka, H. *J. Comput. Chem.* **2007**, *28*, 1735.
- (16) Meeto, W.; Suramitr, S.; Vannarat, S.; Hannongbua, S. *Chem. Phys.* **2008**, *349*, 1.
- (17) Suramitr, S.; Meeto, W.; Wolschann, P.; Hannongbua, S. *Theor. Chem. Acc.* **2010**, *125*, 35.
- (18) Nakatsuji, H.; Hirao, K. *J. Chem. Phys.* **1978**, *68*, 2053.
- (19) Nakatsuji, H. *Chem. Phys. Lett.* **1978**, *59*, 362.
- (20) Nakatsuji, H. *Chem. Phys. Lett.* **1979**, *67*, 329.
- (21) Nakatsuji, H. *Acta Chim. Hung.* **1992**, *129*, 719.
- (22) Nakatsuji, H. SAC-CI method: Theoretical aspects and some recent topics. *Computational Chemistry, Review of Current Trends*; World Scientific: Singapore, 1997.
- (23) Ehara, M.; Hasegawa, J.; Nakatsuji, H. SAC-CI Method Applied to Molecular Spectroscopy. *Theory and Applications of Computational Chemistry: The First 40 Years*; Elsevier: Oxford, U.K., 2005.
- (24) Poolmee, P.; Ehara, M.; Hannongbua, S.; Nakatsuji, H. *Polymer* **2005**, *46*, 6474.
- (25) Poolmee, P.; Hannongbua, S. *J. Comput. Chem.* **2010**, *31*, 1945.
- (26) Saha, B.; Ehara, M.; Nakatsuji, H. *J. Phys. Chem. A* **2007**, *111*, 5473.
- (27) Promkatkaew, M.; Suramitr, S.; Monhaphda, T. K.; Namuangruk, S.; Ehara, M.; Hannongbua, S. *J. Chem. Phys.* **2009**, *131*, 2243060.
- (28) Fukuda, R.; Nakatsuji, H. *J. Chem. Phys.* **2008**, *128*, 094105.
- (29) Fukuda, R.; Ehara, M.; Nakatsuji, H. *J. Chem. Phys.* **2010**, *133*, 144316.
- (30) Tomasi, J.; Mennucci, B.; Cammi, R. *Chem. Rev.* **2005**, *105*, 2999.
- (31) Cammi, R.; Corni, B.; Mennucci, B.; Tomasi, J. *J. Chem. Phys.* **2005**, *122*, 104513.
- (32) Corni, S.; Cammi, R.; Mennucci, B.; Tomasi, J. *J. Chem. Phys.* **2005**, *123*, 134512.
- (33) Caricato, M.; Mennucci, B.; Tomasi, J.; Ingrossi, F.; Cammi, R.; Corni, S.; Scalmani, G. *J. Chem. Phys.* **2006**, *124*, 124520.
- (34) Improta, R.; Barone, V.; Scalmani, G.; Frisch, M. J. *J. Chem. Phys.* **2006**, *125*, 54103.
- (35) Improta, R.; Scalmani, G.; Frisch, M. J.; Barone, V. *J. Chem. Phys.* **2007**, *127*, 74504.
- (36) Scalmani, G.; Frisch, M. J.; Mennucci, B.; Tomasi, J.; Cammi, R.; Barone, V. *J. Chem. Phys.* **2006**, *124*, 094107.
- (37) Cammi, R.; Fukuda, R.; Ehara, M.; Nakatsuji, H. *J. Chem. Phys.* **2010**, *133*, 024104.
- (38) Fukuda, R.; Ehara, M.; Nakatsuji, H.; Cammi, R. *J. Chem. Phys.* **2011**, *133*, 144316.
- (39) Becke, A. D. *Phys. Rev. A* **1988**, *38*, 3098.
- (40) Lee, C.; Yang, W.; Parr, R. G. *Phys. Rev. B* **1988**, *37*, 785.
- (41) Becke, A. D. *J. Chem. Phys.* **1993**, *98*, 5648.
- (42) Perdew, J. P.; Burke, K.; Ernzerhof, M. *Phys. Rev. Lett.* **1996**, *77*, 3865.
- (43) Perdew, J. P.; Burke, K.; Ernzerhof, M. *Phys. Rev. Lett.* **1997**, *78*, 1396.
- (44) Zhao, Y.; Truhlar, D. G. *J. Phys. Chem. A* **2006**, *110*, 13126.
- (45) Dunning, T. H., Jr.; Hay, P. J. In *Modern Theoretical Chemistry*; Schaefer, H. F., III, Ed.; Plenum: New York, 1976; Vol. 3.
- (46) Yanai, T.; Tew, D. P.; Handy, N. C. *Chem. Phys. Lett.* **2004**, *393*, 51.
- (47) Nakatsuji, H. *Chem. Phys.* **1983**, *75*, 425.
- (48) Frisch, M. J.; Trucks, G. W.; Schlegel, H. B.; Scuseria, G. E.; Robb, M. A.; Cheeseman, J. R.; Scalmani, G.; Barone, V.; Mennucci, B.; Petersson, G. A.; et al. *GAUSSIAN 09*, revision B.01.; Gaussian Inc.: Wallingford, CT, 2010.
- (49) Mennucci, B.; Cammi, R.; Tomasi, T. *J. Chem. Phys.* **1998**, *106*, 2798.
- (50) Kongsted, J.; Osted, A.; Mikkelsen, K. V.; Christiansen, O. *Mol. Phys.* **2002**, *100*, 1813.
- (51) Gabanski, R.; Waskiewicz, K.; Suwinski, J. *ARKIVOC* **2005**, 58.
- (52) Liu, Q.; Liu, W.; Yao, B.; Tian, H.; Xie, Z.; Geng, Y.; Wang, F. *Macromolecules* **2007**, *40*, 1851.
- (53) Yang, L.; Ren, A.-M.; Feng, J.-K.; Wang, J.-F. *J. Org. Chem.* **2005**, *70*, 3009.
- (54) Wang, J.-F.; Feng, J.-K.; Ren, A.-M.; Li, Z.-D.; Ma, Y.-G.; Lu, P.; Zhang, H.-X. *Macromolecules* **2004**, *37*, 3451.